http://dx.doi.org/10.5012/bkcs.2012.33.7.2133

Articles

A Newly Designed a TiO_2-Loaded Spherical ZnS Nano/Micro-Composites for High Hydrogen Production from Methanol/Water Solution Photo-Splitting

Jieun Kim and Misook Kang*

Department of Chemistry, College of Science, Yeungnam University, Gyeongsan, Gyeongbuk 712-749, Korea
**E-mail: mskang@ynu.ac.kr*
Received October 18, 2011, Accepted January 6, 2012

A new system using TiO_2 (nano-sized, band-gap 3.14 eV)-impregnated spherical ZnS (micro-sized, band-gap 2.73 eV) nano/micro-composites (Ti 0.001, 0.005, 0.01, and 0.05 mol %/ZnS) was developed to enhance the production of hydrogen from methanol/water splitting. The ZnS particles in a spherical morphology with a diameter of about 2-4 mm which can absorb around 455 nm were prepared by hydrothermal method. This material was used as a photocatalyst with loading by nano-sized TiO_2 (20-30 nm) for hydrogen production. The evolution of H_2 from methanol/water (1:1) photo splitting over the TiO_2/ZnS composite in the liquid system was enhanced, compared with that over pure TiO_2 and ZnS. In particular, 1.2 mmol of H_2 gas was produced after 12 h when 0.005 mol % TiO_2/ZnS nano/micro-composite was used. On the basis of cyclic voltammeter (CV) and UV-visible spectrums results, the high photoactivity was attributed to the larger band gap and the lower LUMO in the TiO_2/ZnS composite, due to the decreased recombination between the excited electrons and holes.

Key Words : TiO_2/ZnS nano/micro-composite, Hydrogen production, Methanol/water photo-splitting, Band gap

Introduction

ZnS is an important wide band gap (about 2.7 eV) semiconductor which continues to gain attention in recent years in view of its application potential in photo-electronic devices such as light emitting diodes,[1] flat panel displays,[2] nonlinear optical devices,[3] sensors,[4] lasers[5] and photocatalysis.[6-13] ZnS has two different phases, the hexagonal wurtzite phase and the cubic structure phase, and the hexagonal wurtzite phase has been more researched widely because their many usages. Initially, most studies were then focused on synthesis of the ZnS, and thus nano-spherical particles,[14] nanorods,[15] mesoporous,[16] hallow sphere,[17] and nano-plates and nano-belts[18] were synthesized in a variety of shapes. Recently, study of nanocrystalline ZnS is important since the properties like optical absorption and luminescence can be altered by controlling the sizes and morphologies of the material. On introducing dopants, as like Ti,[19] In,[20] Ni,[21] Cu[22] *etc*, defect levels can be created in the band gap which can lead to luminescence in these materials.

In recent years, research on metal sulfide photocatalysts has progressed to applications[23-25] in a new photocatalytic reaction mechanism, because of their narrow band gaps that possibly allow absorption of longer wavelengths, unlike the conventional metal oxide semiconductor systems. Particularly, Muruganandham *et al*.[26] had controlled mesoporous self-assembly of ZnS micro sphere for photocatalytic degradation of methyl orange dye. The catalytic recyclability experiments for degradation of methyl orange showed that mesoporous ZnS micro spheres are easily recyclable when compared to commercial ZnS and TiO_2. Otherwise, hydrogen is likely to become an increasingly used energy source due to its environmental friendliness. The technology for generating hydrogen by the splitting of water using a photocatalyst has attracted considerable attention. The photocatalytic formation of hydrogen and oxygen on semiconductors such as $MTiO_3$[27-29] has been studied extensively due to the low band gap and high corrosion resistance of these semiconductor materials. However, the photocatalytic decomposition of water on a TiO_2 photocatalyst is ineffective because the amount of hydrogen produced is limited by the rapid recombination of holes and electrons, resulting in the formation of water. Yuexiang *et al*.[30] reported that photoactivity of hydrogen generation over Pt/ZnS-$ZnIn_2S_4$ was improved notably with simultaneous degradation of glucose. A large number of OH radicals generated in ZnS-$ZnIn_2S_4$ system, have been tested. However, hydrogen production has not been sufficiently researched on ZnS photocatalysts.

In this study, spherical ZnS micro-particle is synthesized by hydrothermal method using sodium sulfate as a sulfur source and a minimum TiO_2 precursor is loaded on the materials. The relationship between the spectroscopic properties of the particles and the catalytic performance for the production of H_2 over the TiO_2 /ZnS nano/micro-composites

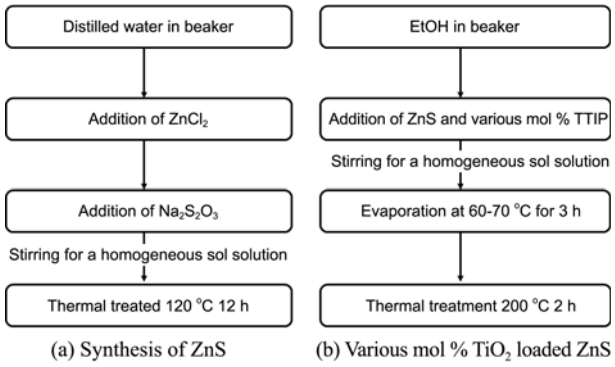

Figure 1. Preparation of ZnS and TiO_2/ZnS nano/micro composites by a conventional hydrothermal process and impregnation method.

is examined by X-ray diffraction analysis (XRD), scanning electron microscopy (SEM), UV-visible spectroscopy, photoluminescence spectroscopy, and cyclic voltammeter (CV).

Experimental Section

Synthesis of ZnS and TiO_2/ZnS Nano/Micro Composites. ZnS was prepared using a common hydrothermal method. To prepare the sol mixture, sodium thiosulfate ($Na_2S_2O_3$, 99.9%, Junsei Chemical, Japan) and zinc chloride ($ZnCl_2{\cdot}4H_2O$, 99.9%, Junsei Chemical, Japan) were used as the S and Zn precursors, respectively. 1.0 mole of sodium sulfate was dissolved in water solvent, and 1.0 moles of $ZnCl_2$ was added slowly to the solution and stirred homogeneously for 2 h. The final solution was moved to an autoclave for thermal treatment. Zinc chloride was sulfurized during thermal treatment at 120 °C for 12 h under a nitrogen environment as shown in Figure 1(a). The resulting precipitate was washed with distilled water and then dried at 100 °C for 24 h. The TTIP (titanium tetraisopropoxide, 99.9% Junsei Chemical, Japan) with mole ratios – 0.001, 0.005, 0.01, and 0.05 mol %, this value is the corresponding weight when a TTIP will be converted into a TiO_2 – were added to an ethanol solution containing micro-sized ZnS powder prepared as described in the Figure 1(b). The slurries were milled until the solvent had disappeared completely, and then the powder was thermally treated at 200 °C for 2 h for stable cross linking between TiO_2 and ZnS under air environment. Here, we also prepared an anatase TiO_2 by hydrothermal process to compare with the ZnS catalysts developed in this study. These TiO_2/ZnS nano/micro-composites were used as a photocatalyst for hydrogen production from methanol/water (1:1) photo splitting, and their catalytic performances were compared with those of pure ZnS and TiO_2.

Characteristics of the Synthesized ZnS and TiO_2 /ZnS Nano/Micro Composites. The synthesized ZnS, TiO_2, and TiO_2/ZnS nano/micro composites were examined by XRD (MPD, PANalytical, at Yeungnam University Instrumental Analysis Center) with nickel-filtered Cu Kα radiation (30 kV, 30 mA). The samples were scanned at 2θ angles ranging from 10 to 80° at a scan speed of 10° min^{-1} and a time constant of 1 s. The sizes and shapes of the ZnS, TiO_2, and TiO_2/ZnS nano/micro composites were examined by SEM on SEM-S-4100 (Hitachi, Yeungnam University Instrumental Analysis Center) instrument. The UV-visible spectra were obtained using a NEOSYS-2000 spectrometer (Scinco, Korea) with a reflectance sphere. The CV results were obtained using a BAS 100B at room temperature and a scan rate of 100 mV/s with 0.1M KCl as the supporting electrolyte, a platinum wire as the working and counter electrodes, and Ag/AgCl as the reference electrode. PL spectroscopy was also performed to determine the number of photo-excited electron-hole pairs using a PL mapping system (LabRam HR, Jobin Yvon, French, Korea Photonics Technology Institute Material Characterization Center), and to examine the number of photo-excited electron-hole pairs for all samples. Samples of 1.0-mm pellets were measured at room temperature using a He-Cd laser source at 325 nm in the reflection mode.

Hydrogen Production from Photo Splitting of Methanol/Water. The photo splitting of methanol/water was carried out using a liquid photoreactor designed in our laboratory [31] water photo splitting, 0.5 g of the powdered ZnS, TiO_2, and TiO_2/ZnS nano/micro composites photocatalysts were added to 1.0-L of distilled water in a 2.0-L Pyrex reactor. UV-lamps (6 × 3 W cm^{-2} = 18 W cm^{-2}, 30 cm length × 2.0 cm diameter; Shinan com., Korea) emitting radiation at 365 nm were used. Water photo splitting was carried out for 58 h with constant stirring. Hydrogen evolution was measured after 1 h. The hydrogen gas (H_2) produced during water photo splitting was analyzed using a TCD-type gas chromatograph (GC, model DS 6200; Donam Instruments Inc., Korea). To determine the products and intermediates, the GC was connected directly to the water decomposition reactor. The following GC conditions were used: TCD detector, Carbosphere column (Alltech, Deerfield, IL, USA), 413 K injection temp, 393 K initial temp., 393 K final temp., and 423 K detector temp.

Results and Discussion

Properties of Synthesized ZnS and TiO_2/ZnS Nano/Micro Composites. Figure 2(a) show the crystallinity and expected ion exchanged site obtained from the XRD patterns of the ZnS, TiO_2 (to compare), and TiO_2/ZnS nano/micro composites. All of the peaks could be indexed as the cubic structure (cell constants a = 5.345 Å, JCPDS Card No. 80-0020). The XRD patterns showed main peaks at 28.91, 48.11, and 57.11°, which were assigned to the (d_{111}), (d_{220}), and (d_{311}) planes, respectively. A shoulder peak at 2θ 26.82 (d_{100}) which assigned to the hexagonal wurtzite phase ZnS (cell constants a = 3.822 Å, c = 6.260 Å; JCPDS Card No. 79-2204) was slightly seen also. These peaks were slightly shifted to the lower two theta value with an increase of Ti amount except at 0.05 mol % TiO_2/ZnS. Therefore, there are no correlation between the amount of Ti added and the unit cell parameter. Scherrer's equation, $t = 0.9\lambda/\beta\cos\theta$, where λ is the wavelength of the incident X-rays, β the full width at

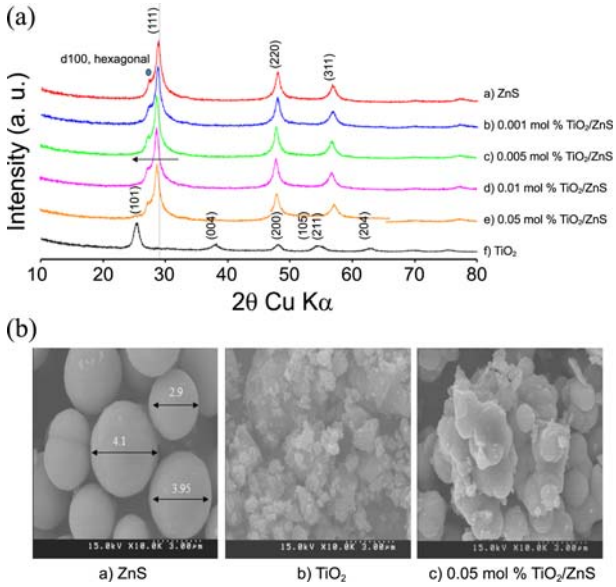

Figure 2. XRD patterns (a) and SEM images (b) of TiO_2, ZnS, and TiO_2/ZnS composites as-synthesized. a) XRD patterns and b) SEM images.

half maximum height in radians, and θ the diffraction angle, was used to estimate the crystalline domain size. This value was 7.57, 6.99, 7.17, 7.62, 7.02, and 6.94 nm for TiO_2, 0.05 mol % TiO_2 /ZnS, 0.01 mol % TiO_2 /ZnS, 0.005 mol % TiO_2 /ZnS, 0.001 mol % TiO_2 /ZnS, and ZnS, respectively. Figure 2(b) shows the low-magnification scanning electron microscopy (SEM) image of the micro-sized ZnS, nano-sized TiO_2, and TiO_2/ZnS nano/micro composite. The morphology of the ZnS product was spherical-like spheres with a diameter of 2-4 mm and, maybe it was expected that a giant three-dimensional micro-particles, ZnS, was formed by the coagulation between the cube-type ZnS nano-sized crystallites together. Otherwise, TiO_2 particles prepared as a comparable sample were located in the range of 20-30 nm and the nano-sized TiO_2 particles are evenly dispersed on the surface of micro-sized ZnS which seen on the TiO_2/ZnS nano/micro composites.

The atomic composition was analyzed by energy-dispersive X-ray spectroscopy (EDS) study (Table 1), which revealed the presence of Zn and S as the only elementary components of the product with a Zn:S atomic ratio = 53:47. The molar ratio of Zn(1) to S(1) obtained from EDS suggests that S is a little less than Zn, but it is still close to the stoichiometric ZnS. On the other hand, TiO_2 also has good crystallinity as an anatase structure with atomic ratio Ti:O=25:75, as induced from EDS in Table 1. In the case of the TiO_2/ZnS nano/micro composite, although there was very little reduction in intensity, the peak positions for the ZnS structure were not changed and no peaks assigned to TiO_2 were observed despite the addition of TiO_2 to the ZnS surface, indicating the high dispersion of the TiO_2 particles into the ZnS surface. The atomic ratio in Table 1 represents the entered actual amounts, in the case of 0.05 mol % TiO_2/ZnS, the Zn:Ti atomic ratio = 2.72:38.91, and however the

Table 1. Atomic composition as analyzed by EDS study

Sample	E_{red} (mV) *vs* Ag/AgCl	LUMO (eV)	Band gap (eV)
ZnS	-1.27	-3.11	2.73
TiO_2	-0.36	-4.02	3.14
0.005 mol % TiO_2/ZnS	-1.12	-3.26	2.81

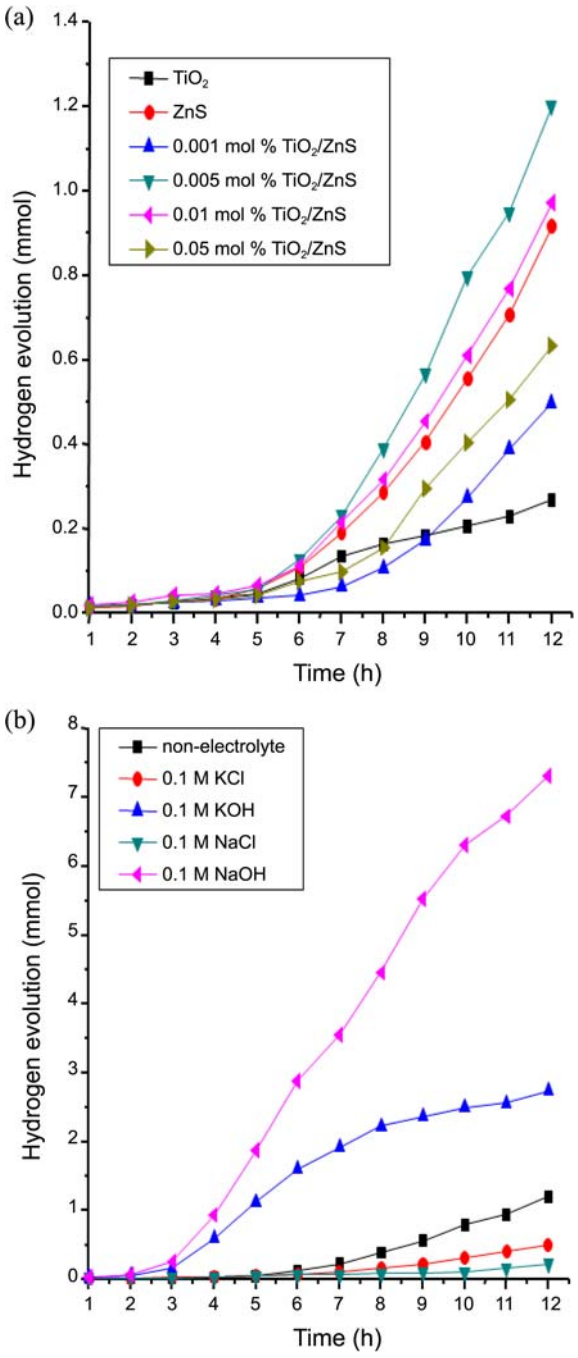

Figure 3. Hydrogen production from methanol/water photo splitting as a function of the reaction time over TiO_2, ZnS, and TiO_2/ZnS composites: (a) according to the types of photocatalyst and (b) the effect of the electrolytes.

Ti component was not observed in other samples, because of the amount is too small.

Hydrogen Production from Methanol/Water Splitting over ZnS Nano/Micro Composites. Figure 3 summarizes the evolution of H_2 from methanol/water (=1) to splitting over the ZnS, TiO_2, and TiO_2/ZnS photocatalysts in a batch-type liquid photo system. In Figure 3(a), a very small amount of H_2 was collected over pure TiO_2 after methanol/water photodecomposition for 12 h, while a significant amount of H_2 gas was collected over the ZnS. Particulary, the hydrogen emission was further increased over TiO_2/ZnS nano/micro-composites: the amount of H_2 produced reached 1. 2 mmol over 0.5 g of the 0.005 mol % TiO_2/ZnS. However, the amount produced was lower on the 0.05 mol % TiO_2/ZnS catalysts with higher TiO_2-loadings. The use of two semiconductors can be considered a promising method to improve charge separations, to increase the lifetime of charge carriers, and to enhance the efficiency of the interfacial charge transfer to adsorbed substrate. For efficient inter-particle electron transfer between the semiconductors that is considered as the sensitizer, ZnS, the conduction band of TiO_2 must be more anodic than the corresponding band of the sensitizer. Under visible irradiation, only the sensitizer, ZnS, is excited, and electrons generated to their conduction band are injected into the inactivated TiO_2 conduction band. These thermodynamic conditions favor the phenomenon of electron injections. Particularly, the catalytic performance for water/methanol decomposition over TiO_2/ZnS was more enhanced in the presence of electrolytes (alkali solutions of 0.1 M, Figure 3(b)). The hydrogen production dramatically increased in the alkali solution to reach 7.4 mmol after 12 h in NaOH solution and also increased similarly in a KOH solution. The following mechanisms[32,33] of three types are presented to explain this result.

I) the photocatalysis over TiO_2/ZnS

$$TiO_2/ZnS + hv \rightarrow TiO_2/ZnS\ (h^+ + e^-) \quad \text{(I-1)}$$

$$TiO_2/ZnS\ (h^+) + CH_3OH \rightarrow TiO_2/ZnS + \cdot CH_2OH + H^+ \quad \text{(I-2)}$$

$$TiO_2/ZnS\ (e^-) + H^+ \rightarrow TiO_2/ZnS + \tfrac{1}{2}H_2\uparrow \quad \text{(I-3)}$$

$$\cdot CH_2OH \rightarrow HCHO + H^+ + e^- \quad \text{(I-4)}$$

$$\cdot CH_2OH + H^+ + e^- \rightarrow CH_3OH \quad \text{(I-5)}$$

$$TiO_2/ZnS\ (h^+) + e^- \rightarrow TiO_2/ZnS \quad \text{(I-6)}$$

The electroactive species such as CH_2OH radical, OH radical and H_2 produced in the reactions (I-2), (I-3) and (I-4) can be oxidized or reduced at biased TiO_2/ZnS catalysts to generate anodic and cathodic photocurrents according to the following anodic reactions (I-5) and (I-6).

II) the effect of alkali solution

$$TiO_2/ZnS\ (OH)x + hv \rightarrow h^+ + \cdot e^-_{cb} \quad \text{(II-1)}$$

$$h^+ + H_2O \rightarrow \cdot OH + H^+ \quad \text{(II-2)}$$

$$h^+ + OH^-(\text{alkali}) \rightarrow \cdot OH \quad \text{(II-3)}$$

$$H^+ + \cdot e^-_{cb} \rightarrow \tfrac{1}{2}H_2\uparrow \quad \text{(II-4)}$$

In basic solution, TiO_2/ZnS(OH), when TiO_2/ZnS (OH)x particles were irradiated, electron hole pairs formed. Valence band holes can be filled by the surface water molecules or hydroxyl ions to form hydroxyl radicals. Electron acceptor H^+ obtains the conduction electron to produce hydrogen because conduction band of TiO_2/ZnS(OH) is negative enough for hydrogen evolution.

III) the effect of sulfur in ZnS

$$\equiv Zn - SH + hv \rightarrow \equiv Zn - SH\cdot\ (h^+ + e^-) \quad \text{(III-1)}$$

$$\equiv Zn - SH\cdot \rightarrow \equiv Zn - S^{2-} + \cdot H \quad \text{(III-2)}$$

$$\equiv Zn - S^{2-} + H^+ \rightarrow \equiv Zn - S^- + \cdot H \quad \text{(III-3)}$$

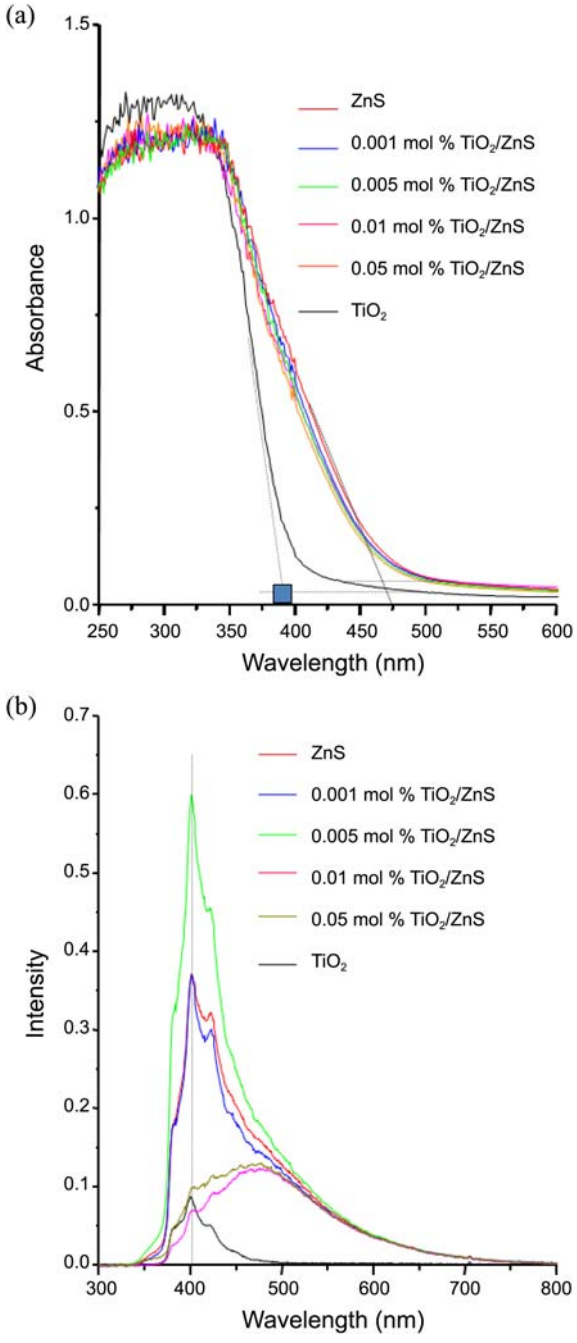

Figure 4. UV-visible (a) and PL spectra (b) of TiO_2, ZnS, and TiO_2/ZnS composites as-synthesized.

$$\cdot H + \cdot H \rightarrow H_2 \uparrow \quad \text{(III-4)}$$

$$\equiv Zn - S^- + e^- \rightarrow \equiv Zn - S^{2-} \quad \text{(III-5)}$$

HS^- and S^{2-} can react with the formed hydroxyl radicals to improve the hydrogen evolution. Because of hydrated radius of S^{2-} ion should be larger than that of HS^- ion, S^{2-} would diffuse more slowly from bulk solution to the photocatalyst surface than HS^-.

Spectroscopic Properties of the Synthesized ZnS and TiO_2/ZnS Nano/Micro Composites. Figure 4 exhibits the UV-visible and PL spectra of the ZnS, TiO_2, and TiO_2/ZnS composite powders. The absorption band for the tetrahedral symmetry of Ti^{4+} normally appears at approximately 380 nm, and is assigned to ligand (p-orbital) to metal (d-orbital) charge transfer in Figure 4(a)). Otherwise, the ZnS was absorbed by all of the visible area, which acted as sulfur in the red color range. The obtained UV spectra of ZnS nano-particles were used for evaluation of the band gap energy by the Tauc relation.[34] The plot revealed the band gap energy of 2.73 eV at 455 nm, and this band gap energy was used for the estimation of ZnS nano-particles size. In the spectra for the TiO_2/ZnS composite, the absorption bands were similar to that of pure ZnS. Generally, the band gap in a semi-conductor material is closely related to the wavelength range absorbed where the band gap decreases with increasing absorption wavelength. Consequently, materials with a narrow band gap can readily be extended for the utilization of visible light, whereas a smaller band gap could reduced the photoactivity by increasing the recombination rate between electrons and holes. The maximum absorptions in the TiO_2/ZnS were gradually shifted to a shorter wavelength compared to those of pure ZnS, with an increase of Ti amount. The band gap obtained by extrapolation in 0.005 mol % TiO_2/ZnS (442 nm) at the meeting point of the two tangents was about 2.81 eV. Figure (b)) shows the PL spectra of the TiO_2, ZnS and TiO_2/ZnS particle. The curve suggests that the electrons in the valence band are transferred to the conduction band, after which the excited electrons are stabilized by photoemission. In general, the PL intensity increases with increasing number of emitted electrons resulting from recombination between excited electrons and holes.[35,36] Therefore, there is a strong relationship between the PL intensity and photoactivity. In particular, the PL intensity decreases to a greater extent when a metal can

Table 2. Comparison of LUMO energies and band gaps for TiO_2, ZnS, 0.005 mol % TiO_2/ZnS composites

Sample	E_{red} (V) *vs* Ag/AgCl	LUMO (eV)	Band gap (eV)
ZnS	-1.27	-3.11	2.73
TiO_2	-0.36	-4.02	3.14
0.005 mol % TiO_2/ZnS	-1.12	-3.26	2.81

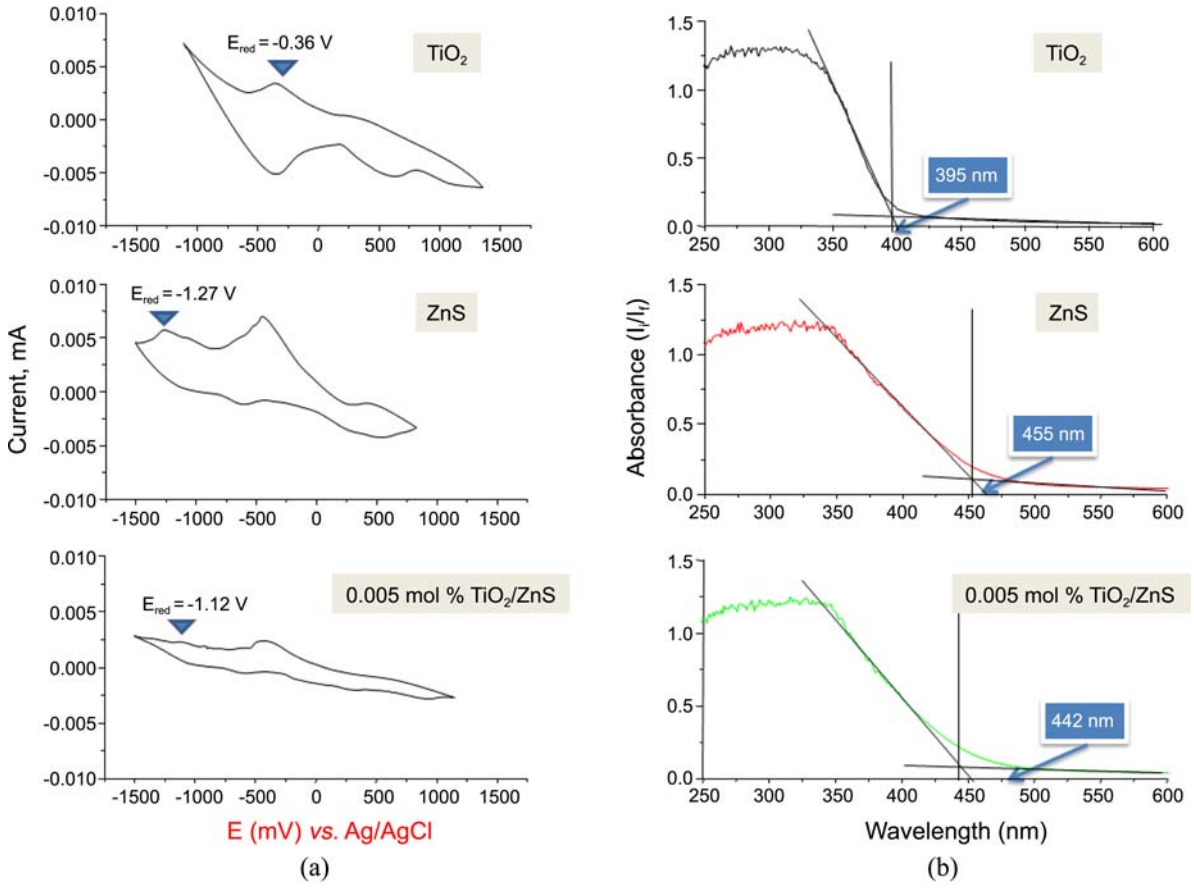

Figure 5. Comparison of CV voltammeter (a) and band gaps (b) for TiO_2, ZnS, 0.005 mol % TiO_2/ZnS composites.

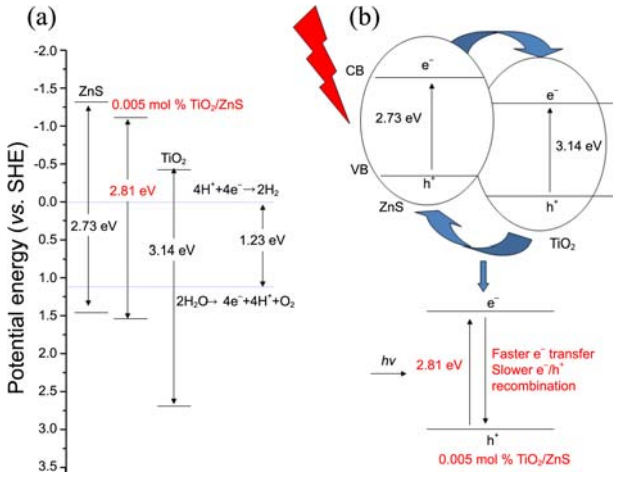

Figure 6. Proposed potential energy diagram (a) and expected models for photocatalytic progress (b) over for TiO_2, ZnS, and TiO_2/ZnS composites.

capture excited electrons or exhibit conductivity, which is known as the relaxation process. The PL curve of the TiO_2 particle exhibit very small at 400 nm compared to ZnS particle. The PL intensity increased dramatically in 0.005 mol % TiO_2/ZnS, due to the effect of its clean surface in facilitating electron transfer and hence increasing the OH radicals on valence band of semiconductor. Consequently, many electron transferring are easily expected on the surface of TiO_2/ZnS. Otherwise, over more TiO_2 loaded catalyst, the PL band was shifted the down field, and it has been broadened. The band broadening is attributed to the overlapped emission from the higher and lower excited states to the ground states.[37]

The utility of the CV results shown in Figure 5 is highly dependent on the analytic condition being studied, and it has to be redox active within the experimental potential window. It is desirable to display a reversible wave, which gives the following information: the reversible reactions display a hysteresis of absolute potential between the reduction (E_{pc}) and oxidation (E_{pa}) peaks. Reversible reactions will show a ratio of the peak currents passed at reduction (i_{pc}) and oxidation (i_{pa}) that is near unity ($1 = i_{pa}/i_{pc}$). When such reversible peaks are observed thermodynamic information in the form of half-cell potential, $E^0_{1/2}$ ($E_{pc}+E_{pa}/2$) can also be determined.[38] Especially when waves are semi-reversible, such as when i_{pa}/i_{pc} is less than or greater than 1, it can be possible to determine more information about the kinetic processes. In this study, the oxidation potentials were measured by means of CV in distilled water solutions of the 0.2 mM complex using a pelletized sample as the working electrode, Ag/AgCl as the reference electrode, and 0.1 M KCl as the supporting electrolyte. The electronic parameters for CV are listed in Table 1. In the synthesized ZnS and TiO_2/ZnS, the $Zn^{2+} \rightarrow Zn^0$ and $Ti^{4+} \rightarrow Ti^{3+}$ redox processes resemble two reversible reactions; however, we could not determine the $S^{2-} \rightarrow S^-$ thermodynamic value of $E^0_{1/2}$ unfortunately. Recently, some researchers have reported a useful equation, which can determine the energy levels of the highest occupied molecular orbital (HOMO) and the lowest unoccupied molecular orbital (LUMO) using CV.[39] First, the ferrocene ($E_{1/2}$ *vs* $_{Ag/Ag^+}$ = +0.42 eV) potential as a standard should be measured in the electrolyte solution using the same reference electrode, and −4.8 eV fixed as an energy level in the vacuum set. Finally the energy levels of HOMO and LUMO can be calculated using the following formula: HOMO (or LUMO) (eV) = $-4.8-(E_{onset} - E_{1/2(Ferrocene)})$. Here, E_{onset} is a starting point of the redox potential, and is used more than the peak potential values. The onset potentials for reduction with the Ag/AgCl reference electrode in ZnS and TiO_2/ZnS are −1.27 and −1.12 eV, respectively, and the LUMO energy levels can therefore be calculated as −3.11 and −3.26 eV, respectively.

We propose the potential energy for TiO_2, ZnS, and TiO_2/ZnS nano/micro composites, as shown in Figure 6(a), based on the results of the CV curve and UV-visible spectra. The band gap of ZnS was smaller than TiO_2, and therefore, the electrons on the valence band are easily transferred into the conduction band although with a weaker energy. Consequently, the photocatalytic activity was enhanced over the ZnS composite compared to TiO_2, with the fast initial emission. Otherwise, the band gap of the TiO_2/ZnS composite was slightly wider than that of pure ZnS, and its valence and conduction bands were at higher and lower energy levels, respectively, than those of ZnS. This result means that the excited electrons from the valence band during photocatalysis were recombined with the holes slowly, which allowed the hole effect at the valence band to continue for a longer time than that for pure ZnS. Note should be made of the other peak in the CV results, *i.e.*, the redox peak of ZnS at $E_{red} = -1.27$ eV. This means that isolated ZnS partially presents differently from the TiO_2/ZnS composite. Despite the incomplete presence of ZnS, the photocatalytic performance was better in the TiO_2/ZnS composite. This difference is explained by a model shown in Figure 6(b). If ZnS and TiO_2 are separated, the first electronic transition occurs in the two semiconductors by the UV radiation source, and then the electrons at a higher conduction band in ZnS move onto the TiO_2 conduction band, whereas the hole in TiO_2 moves to the valence band of ZnS, which is formed by the current recycle. Therefore, their recombination of excited electrons and holes will be suppressed during photocatalysis. These phenomena consequently increase the evolution of OH radicals formed from the electrons and holes, and the rate of degradation of methanol and water will eventually enhance the photocatalytic performance. Meanwhile, the TiO_2/ZnS composite was perfectly formed the combination between TiO_2 and ZnS, together the initial photoreaction was faster because a shorter band gap than over TiO_2, and the recombination of electrons and holes was slower than over ZnS, thus raising the catalytic performance. The TiO_2/ZnS co-catalyst exhibited better catalytic performance than the TiO_2 and ZnS monocatalysts.

Conclusions

Micro-sized ZnS was synthesized by hydrothermal method, and was loaded at four different molar ratios by nano-sized TiO_2 for photocatalysis. The morphology of the ZnS particles was shown in the SEM image as spherical spheres with a diameter of 2-4 mm. It was revealed in the UV-visible spectra and CV results that the band gap in pure ZnS and 0.005 mol % TiO_2/ZnS was about 2.73 and 2.81 eV, and the LUMO energy levels were calculated as −3.11 and −3.26 eV, respectively. On the basis of these spectroscopic properties, a significant amount of H_2 gas was collected over the TiO_2/ZnS composites, peaking at 1.2 mmol over 0.005 mol % TiO_2/ZnS. The hydrogen production dramatically increased in alkali solution to reach 7.4 mmol after 12 h in NaOH solution. We attributed this higher catalytic performance over the TiO_2/ZnS composites to the faster electron transferring and slower recombination of electrons and holes.

Acknowledgments. This work was supported by the National Research Foundation of Korea (NRF) grant funded by the Korea government (MEST) (No. 2011-0003286), for which the authors are very grateful.

References

1. Nakamura, S.; Yamada, Y.; Taguchi, T. *J. Cryst. Growth* **2000**, *214/215*, 1091.
2. Liu, X.; Cai, X.; Mao, J.; Jin, C. *Appl. Surf. Sci.* **2001**, *183*, 103.
3. Nazerdeylami, S.; Saievar-Iranizad, E.; Dehghani, Z.; Molaei, M. *Physica B* **2011**, *406*, 108.
4. Luo, L.; Chen, H.; Zhang, L.; Xu, K.; Lv, Y. *Analytica Chimica Acta* **2009**, *635*, 183.
5. Yano, S.; Schroeder, R.; Ullrich, B.; Sakai, H. *Thin Solid Films* **2003**, *423*, 273.
6. Liu, Y.; Hu, J.; Ngo, C.; Prikhodko, S.; Kodambaka, S.; Li, J.; Richard, R. *Appl. Catal. B: Environ.* **2011**, *106*, 212.
7. Franco, A.; Neves, M. C.; Ribeiro Carrott, M. M. L.; Mendonc, M. H.; Pereira, M. I.; Monteiro, O. C. *J. Hazardous Mater.* **2009**, *161*, 545.
8. Kho, R.; Torres-Martínez, C. L.; Mehra, R. K. *J. Colloid. Interf. Sci.* **2000**, *227*, 561.
9. Shao, M.; Han, J.; Wei, M.; Evans, D. G.; Duan, X. *Inter. J. Hydro. Energy* **2011**, *36*, 13452.
10. El-Kemar, M.; El-Shamy, H. *J. Photochem. Photobiol. A: Chem.* **2009**, *205*, 151.
11. Li, Y.; He, F.; Peng, S.; Lu, G.; Li, S. *Inter. J. Hydro. Energy* **2011**, *36*, 10565.
12. Torres-Martínez, C. L.; Kho, R.; Mian, O. I.; Mehra, R. K. *J. Colloid Interf. Sci.* **2001**, *240*, 525.
13. Chen, J.; Lin, S.; Yan, G.; Yang, L.; Chen, X. *Catal. Commun.* **2008**, *9*, 65.
14. Song, H.; Leem, Y.-M.; Kim, B.-G.; Yu, Y.-T. *J. Phys. Chem. Solids* **2008**, *69*, 153.
15. Feng, Q. J.; Shen, D. Z.; Zhang, J. Y.; Liang, H. W.; Zhao, D. X.; Lu, Y. M.; Fan, X. W. *J. Cryst. Growth* **2005**, *285*, 561.
16. Zhang, W.-M.; Li, H.-M.; Sun, Z.-X.; Zhang, Q.; Forsling, W. *Microporous Mesoporous Mater.* **2012**, *147*, 222.
17. Shao, H.-F.; Qian, X.-F.; Zhu, Z.-K. *J. Solid State Chem.* **2005**, *178*, 3522.
18. Aleman, B.; Fernandez, P.; Piqueras, J. *J. Cryst. Growth* **2010**, *312*, 3117.
19. Yang, P.; Lü, M.; Xu, D.; Yuan, D.; Song, C.; Zhou, G. *Appl. Phys. A* **2002**, *74*, 525.
20. Zhou, J.; Goto, H.; Sawaki, N.; Akasaki, I. *J. Appl. Phys.* **1986**, *25*, 1663.
21. Soni, H.; Chawda, M.; Bodas, D. *Mater. Lett.* **2009**, *63*, 767.
22. Saravana Kumar, S.; Abdu lKhadar, M.; Nair, KGM. *J. Luminescence* **2011**, *131*, 786.
23. Sharman, R.; Bisen, D. P.; Dhoble, S. J.; Brahme, N.; Chandra, B. P. *J. Luminescence* **2011**, *131*, 2089.
24. Borse, P. H.; Vogel, W.; Kulkarni, S. K. *J. Colloid Interf. Sci.* **2006**, *293*, 437.
25. Tang, T.-P. *Ceramics Inter.* **2007**, *33*, 1251.
26. Muruganandhama, M.; Amuthaa, R.; Repo, E.; Sillanpaa, M.; Kusumoto, Y.; Abdulla-Al-Mamun, M. *J. Photochem. Photobiol. A: Chem.* **2010**, *216*, 133.
27. Hong, W. J.; Kang, M. *Mater. Lett.* **2006**, *60*, 1296.
28. Lee, B.-Y.; Park, S.-Y.; Kang, M.; Lee, S.-C.; Choung, S.-J. *Appl. Catal. A: Gen.* **2003**, *253*, 371.
29. Xu, S.; Ng, J.; Zhang, X.; Bai, H.; Sun, D. D. *Inter. J. Hydro. Energy* **2010**, *35*, 5254.
30. Li , Y.; Wang, J.; Peng, S.; Lu, G.; Lu, S. *Inter. J. Hydro. Energy* **2010**, *35*, 7116.
31. Kwak, B. S.; Chae, J.; Kim, J.; Kang, M. *Bull. Korean Chem. Soc.* **2009**, *30*, 1047.
32. Li, Y.; He, F.; Peng, S.; Lu, G.; Li, S. *Inter. J. Hydro. Energy* **2011**, *36*, 10565.
33. Lin, Y.; Lin, R.; Yin, F.; Xiao, X.; Wu, M.; Gu, W.; Li, W. *J. Photochem. Photobiol. A: Chem.* **1999**, *125*, 135.
34. Rusdi, R.; Rahman, A. A.; Mohamed, N. S.; Kamarudin, N.; Kamarulzaman, N. *Powder Technol.* **2011**, *210*, 18.
35. Kwak, B. S.; Choi, H.-C.; Woo, J. W.; An, J. B.; Ryu, S. G.; Kang, M. *Clean Technol.* **2011**, *17*, 78.
36. Liu, H.; Zhang, K.; Jing, D.; Liu, G.; Guo, L. *Inter. J. Hydro. Energy* **2010**, *35*, 7080.
37. Onishi, T.; Abe, K.; Miyoshi, Y.; Wakita, K.; Sato, N.; Mochizuki K. *J. Phys. Chem. Solids* **2005**, *66*, 1947.
38. Karami, H.; Kafi, B.; Mortazavi, S. N. *Int. J. Electrochem. Sci.* **2009**, *4*, 414.
39. Kim, Y.; Jeong, J. H.; Kang, M. *Inorganica Chimica Acta* **2011**, *365*, 400.